Climatic Change (2025) 178:29
https://doi.org/10.1007/s10584-025-03872-0

Assessing high-resolution precipitation extremes in Central Asia: evaluation and future projections

Sridhar Gummadi[1] · **Srinivasan Samineni**[1] · **Luis Augusto Becerra Lopez-Lavalle**[1]

Received: 22 August 2024 / Accepted: 24 January 2025

Abstract
The sustainability of ecosystems in Central Asia's semi-arid and arid regions is increasingly threatened by anthropogenic climate change, with shifts in extreme precipitation events playing a pivotal role. Effective adaptation strategies depend on precise forecasting of these changes. This study investigates projected trends in mean and extreme precipitation indices across Central Asia (CA) from 1985 to 2100. Utilizing datasets from the fifth generation of ECMWF Reanalysis (ERA5), the Climate Prediction Center (CPC), and high-resolution National Aeronautics and Space Administration (NASA) Earth Exchange Global Daily Downscaled Projections (NEX-GDDP) derived from Coupled Model Intercomparison Project Phase 6 (CMIP6) models, we analyzed four Shared Socioeconomic Pathway (SSP) scenarios across three distinct time periods. The CMIP6 Multi-Model Ensemble (MME) accurately simulates mean annual precipitation (ANP) for much of the region, though it underperforms in mountainous areas. Specifically, it underestimates days with precipitation exceeding 10 mm (PD10MM) and the Simple Daily Intensity Index (SDII) while overestimating Consecutive Dry Days (CDD) in regions with higher altitudes and more precipitation. Projections indicate a potential increase in mean ANP by up to 50% across most of Central Asia, becoming especially prominent from the mid-century onward. Extremes in precipitation, such as the SDII, the maximum 1-day precipitation amount (RX1DAY), and days with over 10 mm of rainfall, are expected to rise in frequency and intensity across the region. In contrast, while CDD may decrease in eastern CA, it will likely increase in the west by the century's end. These anticipated changes suggest increased wetness under warming scenarios, with more frequent heavy precipitation events and a reduction in prolonged dry periods, particularly under high-emission pathways. The data provides a foundation for developing effective adaptation strategies to enhance resilience against the impacts of climate change in Central Asia.

✉ Sridhar Gummadi
s.gummadi@biosaline.org.ae

[1] International Center for Biosaline Agriculture (ICBA), Dubai, UAE

Published online: 05 February 2025

1 Introduction

Central Asia (CA) comprises predominantly semi-arid to arid regions that are especially vulnerable to the current climate variability and projected future climate change. The fragile ecosystems of this region are significantly sensitive to shifts in climate patterns, influenced by both natural factors and human-induced greenhouse gas emissions (GHGs). These changes pose considerable threats to agricultural systems, food security, water resources, and natural environments, livelihoods, human health, crop and livestock production across the region. Moreover, the exacerbation of extreme climate events, such as droughts, floods, and heat waves, due to global warming, can result in devastating impacts on natural ecosystems. Studies have indicated a marked increase in the frequency and magnitude of extreme climate events over the past two decades correlating with human-influenced GHGs (Alexander et al. 2006; Westra et al. 2013; Zhang et al. 2013; Kim et al. 2016; Stott 2016; Donat et al. 2016; Yao et al. 2021;).

Given the potential impacts of extreme events, there is a growing interest in predicting these events using Earth System Models (ESMs) as a primary tool. However, the projected changes in precipitation, particularly extremes, exhibit high uncertainty. Evaluating historical precipitation events simulated by ESMs is essential to enhance confidence in these projections. Several initiatives have assessed the effectiveness of General Circulation Models (GCMs) in simulating precipitation patterns at both global and regional levels (McMahon et al. 2015; Du et al. 2022) including studies focusing on the Indian subcontinent (Jain et al. 2019; Gusain et al. 2020) and across Central Asia (Zhang et al. 2019; Dong and Dong 2022; Liu et al. 2022). These evaluations provided valuable insights for researchers, highlighting the challenges of these simulations for impact studies and informing policymakers. Clear uncertainties have been identified in the precipitation simulations of the CMIP5. For instance, the consecutive dry days (CDD) and precipitation intensity over Eastern and Southern Africa were underestimated (Ayugi et al. 2022), while the precipitation intensity and frequency of rainy days were overestimated in the northern parts of the United States (Agel et al. 2020). Similarly, CMIP5 models overestimated the interannual variability in precipitation across central Asia (Ta et al. 2018).

According to the latest IPCC assessment report (IPCC 2022), global average surface temperatures are anticipated to exceed or equal 1.5 °C by 2050, underscoring the urgency of addressing climate change impacts. The rising GHGs have resulted in unusual warming of the earth leading to increased extreme events. The increased GHGs are expected to have different impacts at the regional scale, where the projected climate might have different impacts on the local natural ecosystems. Over the past decade, various regions around the world have witnessed a significant rise in the frequency of extreme precipitation events, posing threats to food security, livelihoods, and potentially leading to cross-border conflicts (Carter et al. 2021).

Central Asia, a region highly impacted by climate change, has witnessed an increase in extreme events such as droughts, floods, heat waves, and the drying of the Aral Sea (Chevallier et al. 2014; Kenzhebaev et al. 2017; Fallah et al. 2023). The significant shrinkage of the Aral Sea has affected the continental climate of Central Asia, intensifying local extremes. As a result, summers have become hotter, drier, and longer, while winters have also experienced a trend toward drier conditions. These changes have had profound effects on the region's ecological, social, agricultural, and economic stability and have impacted human health due

to pollution in drinking water sources(Narbayep and Pavlova 2022). With the loss of the Aral Sea's geochemical runoff regulation, surrounding areas now experience aeolian salt transport. Global paleogeographic studies indicate that arid and semi-arid regions, including Central Asia, are particularly susceptible to rapid hydrological, geomorphological, and biological shifts in response to climate change (Varushenko 1987; Goudie Andrew 1994; Lioubimtseva et al. 1998). Projections from advanced CMIP6 models suggest that, under high-emission scenarios, Central Asia may experience a reversal in these trends by the end of the 21st century. The models indicate a shift towards a rising wetness trend, characterized by increased mean precipitation and more frequent extreme precipitation events, particularly in high-emission scenarios. This study utilizes NASA NEX-GDDP CMIP6 models to assess how well these projections capture Central Asia's spatiotemporal precipitation patterns and extremes. The results offer valuable insights for hydrological, agricultural, and resource management studies, supporting more informed decision-making and the development of location-specific adaptation strategies for the sustainable management of natural resources.

2 Data and methods

2.1 Study area

Five nations constitute Central Asia, situated in the centre of Eurasia: Kyrgyzstan, Kazakhstan, Tajikistan, Turkmenistan, and Uzbekistan. These countries have geomorphological landscapes primarily consisting of grasslands and deserts. The continental interior region is challenging for marine air currents to penetrate due to its inland location. The impact of marine influence on CA is minimal due to the Pamir Plateau and the Tien Shan mountains acting as barriers blocking moisture from the Pacific and Indian Oceans. Instead, the region is mostly influenced by westerly winds. Due to the prevalence of westerly circulation, the Atlantic and Arctic oceans are the primary sources of moisture. The region experiences wide variations in precipitation, with basins and plains (rain shadow zones) receiving 150 mm of precipitation annually and mountainous areas with windward slopes receiving 1500 mm (Fig. 1). Due to the rain shadows created by tall mountain ranges, a significant portion of Central Asia's landmass has an arid or semi-arid climate (Lioubimtseva and Cole 2006). This arid-semiarid climate experiences temporal and geographical fluctuations influenced by the region's diverse topography. The temperate continental climate of CA is characterized by dryness, strong evaporation, and abrupt temperature variations (Lioubimtseva and Henebry 2009; Li et al. 2015). The region is particularly vulnerable to climate change because of its location and limited rainfall.

2.2 Data

Primarily, the CMIP6 models were evaluated for their accuracy in reproducing historical climate trends across various time periods and geographic locations. For the evaluation of thirty statistically downscaled and bias-corrected precipitation datasets (0.25° x 0.25°) from the NEX-GDDP project database, only CPC and ERA5 data were used. This selection was made to scrutinize precipitation variability and extremes, considering the extensive avail-

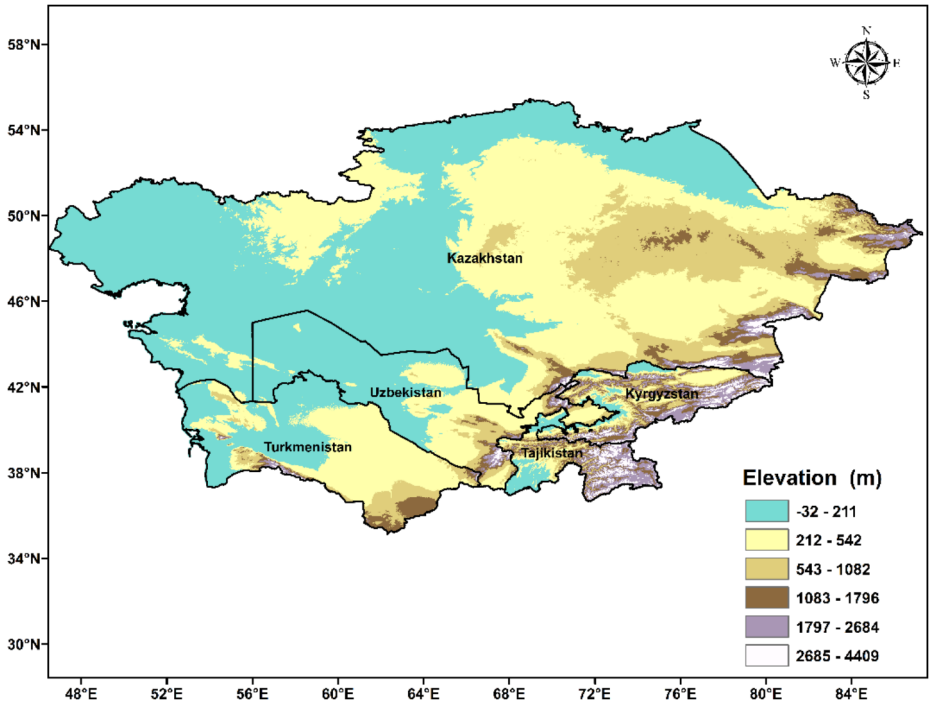

Fig. 1 Topographic features of the Central Asian countries

ability of daily precipitation records. Meanwhile, monthly datasets such as GPCC and CRU assessed the spatial and temporal distribution of monthly precipitation across Central Asia.

2.2.1 Assimilated gridded precipitation products

The ERA5(Hersbach et al. 2020) precipitation dataset, a fifth-generation atmospheric reanalysis developed by the ECMWF in 2020, offers a complete overview of global climate from January 1950 to the present. This dataset was used to analyse the spatial-temporal precipitation patterns across Central Asia. The ERA5 is widely adopted for observational studies globally and serves as a valuable resource, especially in regions with limited gauge data availability. The high-resolution ERA5 datasets were generated from the forecasts (HRES) at a 31-kilometer resolution. ERA5 accurately captures atmospheric dynamics with 137 levels from the surface up to an altitude of 80 km. Access to the ERA5 data is available for download at https://www.ecmwf.int/en/forecasts/datasets/reanalysisdatasets/era5.

The Climate Prediction Center (CPC), a division of the National Oceanic and Atmospheric Administration (NOAA), provides daily precipitation data at a spatial resolution of 0.25° × 0.25° from 1979 to 2022. This dataset is crucial for understanding the observed variability. CPC constructed this dataset through optimal interpolation of quality-controlled gauge records from the Global Telecommunication System (GTS) network (Fan and van den Dool 2008; Chen et al. 2008; Harris et al. 2014). These observations undergo rigorous quality control procedures to ensure reliability. The quality control process involves a com-

prehensive examination of station data. Further details regarding data development can be found on the CPC website at https://psl.noaa.gov/data/gridded/.

A widely used monthly climate dataset, CRU TS (Climatic Research Unit gridded Time Series), uses a 0.5° by 0.5° grid to cover terrestrial areas worldwide, except Antarctica. CRU TS v4 is based on estimated monthly climatic anomalies from large weather station networks (Harris et al. 2014). It incorporates more station data to cover the years 1901–2023, with yearly updates scheduled. Monthly observations from land stations contain seven variables: mean, minimum, and maximum temperatures, precipitation, vapour pressure, wet days, and cloud cover, ensuring regular updates.

The Global Precipitation Climatology Centre (Becker et al. 2013) is a leading source for global precipitation data collected from gauges. The GPCC compiles its gridded product from data provided by 180 institutions, covering approximately 85,000-gauge locations that have recorded observations at least once since 1901. The Full (long-term or climatological) GPCC analysis aims to deliver a high-quality dataset. To maintain continuous precipitation records from individual stations, the GPCC enforces a minimum observation period of 10.

2.2.2 High-resolution model data

The simulated daily high-resolution statistically downscaled precipitation data were sourced from the NASA Earth Exchange Global Daily Downscaled Projections data portal for 33 CMIP6 models (https://nex-gddp-cmip6.s3.us-west-2.amazonaws.com/index.html#NEX-GDDP-CMIP6/) (Xu et al. 2023, 2024). These downscaled climate scenarios cover the historical period from 1950 to 2014 and future projections from 2015 to 2100 on a global scale. These datasets serve as a foundation for evaluating future climate patterns. Derived from state-of-the-art Earth System Models (ESMs) simulations developed under the CMIP6, these datasets utilize the Bias-Correction Spatial Disaggregation (BCSD) method outlined (Wood et al. 2002, 2004; Maurer and Hidalgo 2008; Thrasher et al. 2012, 2022). The information on these NEX- GDDP model datasets is provided in Supplementary Table 1.

The CMIP6 models offer numerous large ensemble members, each distinguished by variant labels indicating realizations (r), initialization (i) schemes, different physics (p), and forcing (f) indices. For the analysis, the initial ensemble member (r1i1p1f1) of the historical simulation, derived from the pre-industrial control simulation of each model, was considered. To present a range of end-of-century climate change projections, a set of scenarios was selected. The scenarios introduced in CMIP6 are referred to as Shared Socioeconomic Pathways (SSPs). They include SSP1-2.6 (low emissions), SSP2-4.5 (medium emissions), SSP3-7.0 (high emissions), and SSP5-8.5 (very high emissions). Historical simulations are driven by aerosols, man-made greenhouse gas emissions, and external natural variables such as solar and volcanic activity. On the other hand, SSP narratives were utilized to facilitate simulations for climate projections extending beyond 2014. Societal development indicators, such as population and economy, have been deliberately adjusted in the latest SSPs. These pathways were designed to respond effectively to radiative forcing and maintain a consistent carbon dioxide concentration over the next century. The twenty-first century was segmented into four distinct periods: the historical era (HP; 1985–2014, 30 years), the near future (NF; 2021–2050, 30 years), the mid-future (MF; 2051–2080, 30 years), and the far future period (FF; 2081–2100, 20 years) to analyse both current climate conditions and future climate change estimates.

2.3 Methods

To ensure uniformity and comparability, data from the CMIP6 model and gridded precipitation products were standardized to the same grid resolution. Re-gridding involves transforming data from one grid resolution to another using the bilinear interpolation method, ensuring compatibility and comparability across different datasets. By calculating the Multi-Model Ensemble (MME), this procedure minimizes the effects of internal variability and successfully mitigates the random errors that are inherent in individual models (Harrison et al. 2019; Brunner et al. 2020).

2.3.1 Extreme precipitation indices

Operating within the framework of the World Meteorological Organization (WMO), the Expert Team on Climate Change Detection and Indicators (ETCCDI) creates a suite of climatic extremes indicators that reflect changes in the frequency, duration, and size of extreme occurrences(Donat et al. 2013; YIN and SUN 2018) In this study, we focus on extreme precipitation indices derived from precipitation data. Table 1 lists the four extreme precipitation climate indicators [number of heavy precipitation days (PD10mm), SDII, maximum 1-day precipitation (RX1day), and consecutive dry days (CDD) that were selected to understand the changes in precipitation extremes based on the ETCCDI. These indices were selected due to their relevance to the study area and their widespread use in analysing observed and simulated climate data globally (Sillmann et al. 2013a, b; Wilson et al. 2022). This study calculated all four precipitation indices annually for each CMIP6 climate model. Subsequently, the MME is computed for both historical and future climate periods. The selected extreme precipitation climate indices were calculated annually to better understand interannual variability in extreme precipitation across the study regions. This approach recognizes that extreme climate indices are most meaningful when analysed annually (Aerenson et al. 2018; Avila-Diaz et al. 2020).

Table 1 List of extreme indices used in the study

Indices	Description	Units
CDD	The Consecutive Dry Days measures the maximum number of consecutive days with no precipitation within a specific period (season/year)	Days
SDII	The Simple Daily Intensity Index measures the average intensity of precipitation on wet days.	mm/day
PD10MM	The Precipitation Days with more than 10 mm measures the number of days within a specific period (season/year) during which the daily precipitation exceeds 10 mm.	Days
RX1DAY	The maximum 1-day precipitation amount measures the highest amount of precipitation that falls in a single day within a specified period (season/year)	mm

2.3.2 Model evaluation methods

The Sen Slope (Sen 1968) was used to calculate the annual trends in precipitation extremes, enabling an understanding of the trends in both historical data and future projections. The Mann-Kendall (MK) test, which is non-parametric, was used to assess the significance of trends (Kendall 1975). At a predetermined level of statistical significance, typically set at $p<0.05$, this statistical test was utilized to assess the significance of trends in the data. The effectiveness of the simulated precipitation indices over the Central Asian countries was measured using four statistical metrics: the Pearson correlation coefficient (CORR), Mean Absolute Error (MAE), Root Mean Square Error (RMSE), and Percent Bias.

$$Bias = \frac{\sum_{i=1}^{n}(Si - Oi)\,x100}{\sum_{i=1}^{n} Oi} \tag{1}$$

where Oi is the value of the observed precipitation, and Si is the simulated precipitation.

$$\mathrm{RMSE} = \sqrt{\frac{\sum_{i=1}^{n}(S_i - O_i)^2}{n-1}} \tag{2}$$

where n is the number of observations, and Si and Oi are the simulated and observed values, respectively.

$$MAE = \frac{1}{n}\sum_{i=1}^{n} \lfloor Si - Oi \rfloor \tag{3}$$

$$CORR = \frac{\sum_{i=1}^{n}(Si - \overline{S})(Oi - \overline{O})}{\sqrt{\sum_{i=1}^{n}\left(Oi - \overline{O}\right)}\sqrt{\sum_{i=1}^{n}\left(Si - \overline{S}\right)}} \tag{4}$$

where Oi is the observed value, Ôi is the mean of observed data, Si is the simulated value, Sî is the mean of simulated.

The term “bias” describes the extent to which an observational dataset either overestimates or underestimates data. While lower values indicate better performance, the RMSE is a common statistical tool for evaluating model performance. The average absolute difference (MAE) between simulated and observed values in a dataset was used to indicate the proximity of predictions to actual values. Lower MAE values indicate a closer model prediction to the actual values. A CORR value of 0 suggests no relationship between the simulated (Si) and observed (Oi) data; in contrast, a value of 1 (or −1) indicates a strong positive (or negative) correlation between the variables.

To gain insight into potential variations in precipitation levels and extreme occurrences, we calculated the relative error (RE) using Eq. 5, as adapted from Gleckler et al. 2008; Scherrer 2011. The RE quantifies the accuracy of modeled values by comparing them to observational data.

$$RE = \frac{Simulation - Observed}{Observed} x\ 100 \tag{5}$$

Where, Simulation and Observed are 30 years average of precipitation and extreme events except for far-future (20 Years).

Furthermore, the comparison between the interannual variability of the simulations and the observations was evaluated using the Interannual Variability Skill Score (IVS) (Gleckler et al. 2008; Scherrer 2011). The IVS quantifies the agreement between the interannual variability patterns of the simulated and observed data.

$$IVS = \left(\frac{STD_m}{STD_o} - \frac{STD_o}{STD_m}\right)^2 \tag{6}$$

The terms STDm and STDo represent the interannual standard deviation of the model simulation and observation, respectively. A lower IVS score suggests that the selected model aligns more closely with the observed interannual variations. IVS, a symmetric measure of variability, quantifies the similarity between interannual variations in simulations and observations.

3 Results

The study results are presented under three main sections: observed variability and extremes, model validation, and future projected changes. Initially, the historical simulations of CMIP6 models are compared against four observed gridded datasets to validate long-term and interannual variability. Subsequently, the model's ability to replicate historical precipitation extremes was assessed. Furthermore, the analysis was extended to examine future projected changes in precipitation amounts and extremes.

3.1 Observed precipitation climatology

Spatial and temporal variations in ANP across CA were investigated over a 43-year period (1979 to 2022) using four gridded datasets: CPC, CRU, GPCC, and ERA5. High-altitude regions, receiving annual rainfall ranging from 1000 to 1500 mm, were notably identified. Particularly, the south-central Pamir Plateau exhibited high mean ANP exceeding 1000 mm (Fig. 2). Both CRU and ERA5 exhibited the highest annual precipitation amounts in the high-altitude regions of CA, while CPC and GPCC (Supplementary Fig. 1) showed similar spatial patterns, with ANP levels≥700 mm/year, as depicted in Fig. 2a. The mean ANP in the region varied from 100 mm in the arid regions to 1500 mm in the mountainous regions. A decreasing trend in ANP was observed with ERA5 data. At the same time, the other three gridded products displayed non-significant increasing trends (Fig. 2e). The trends in spatial precipitation data for the four gridded products are provided in the Supplementary Fig. 1.

The study highlighted the significant spatial and temporal variability and increased standard deviation of ANP patterns. Thus, an in-depth analysis of extreme precipitation events is essential to understand the precipitation patterns across the CA region. We exhibit the precipitation extremes over CA using gridded precipitation data from 1979 to 2022 from

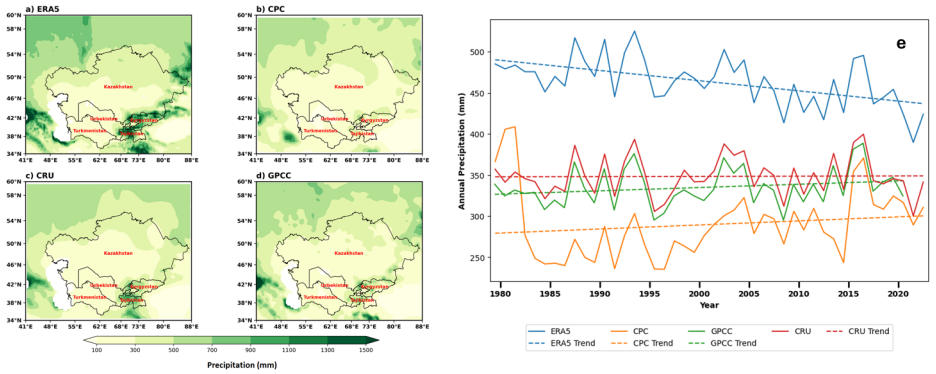

Fig. 2 Central Asian mean ANP climatology pattern, 1979–2022, **a**: ERA5, **b**: CPC, **c**: CRU, and **d**: GPCC. ANP trend during the same time period (**e**)

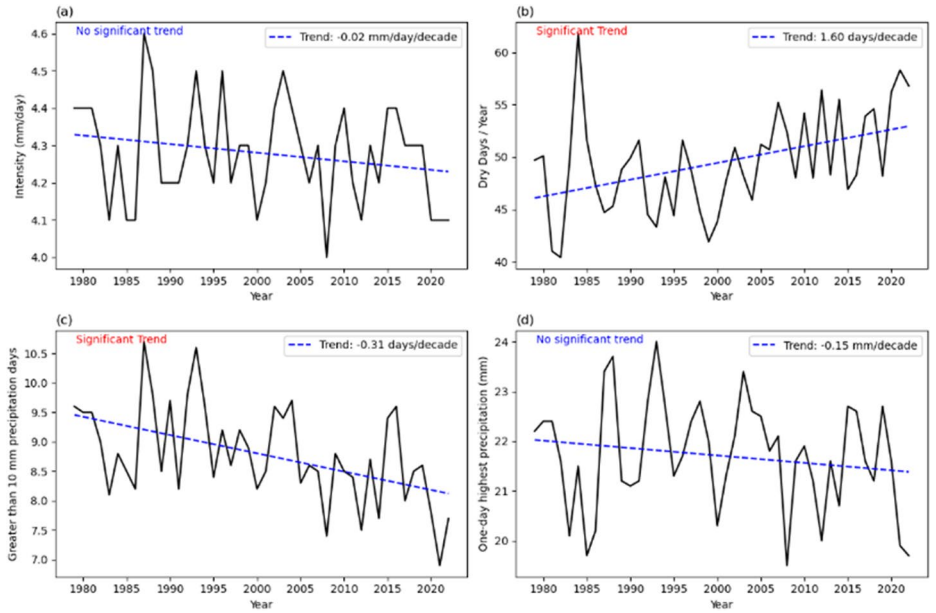

Fig. 3 ERA5 inter-annual variability in **a**: SDII, **b**: CDD, **c**: PD10MM and **d**: RX1DAY precipitation indices over Central Asia. The blue dotted line represents the linear trend observed from 1979 to 2022

CPC and ERA5. The CPC and ERA5 gridded dataset were utilized to calculate the extreme precipitation events (SDII, CDD, PD10MM, and RX1day) to analyse the inter-annual variability and detect any significant patterns in these events. The findings showed substantial declining trends in PD10mm index, while the CDD index exhibited increasing patterns. However, no discernible trends were shown by either the RX1DAY or the SDII indices (Fig. 3). On the other hand, the CPC dataset displayed a significant increase in SDII across CA with no significant trends for RX1Day, PD10MM, and CDD (Supplementary Fig. 2).

3.2 Simulations of historical and future projected changes

We compared the NEX-GDDP CMIP6 models' simulation of historical precipitation data with ERA5 and CPC data. This assessment aims to determine how well these models can simulate mean and extreme precipitation patterns that have been observed. Similarly, three alternative time periods are used to assess the future precipitation mean and extreme precipitation changes, as modeled by the CMIP6 models under four SSPs.

3.2.1 NEX-GDDP-CMIP6 historical simulations

Figure 4 presents the evaluation of the MME annual mean precipitation climatology using ERA5 data for the historical period spanning from 1985 to 2014. The mean precipitation obtained from ERA5 (Fig. 4a) and MME (Fig. 4b), and the bias between the two datasets (Fig. 4c) is presented in Fig. 4. Across CA, the MME tends to underestimate precipitation amounts. The mean precipitation pattern is captured by MME, with a larger bias observed in areas with higher mean precipitation (Fig. 4c). The average yearly precipitation in mountainous and desert regions varied from 100 to 700 mm. The MME showed a bipolar bias, with a dry bias over Kazakhstan's central and western regions and a wet bias over the country's southern and eastern portions and Tajikistan's mountainous regions. Slight dry biases of approximately 15% were observed over Turkmenistan and the central plains of Uzbekistan, indicating an underestimation of precipitation by the MME in those areas. Nonetheless, the biases observed in precipitation patterns can be partially attributed to uncertainties in the observation dataset, owing to the intricate geographic nature of the region. The statistically

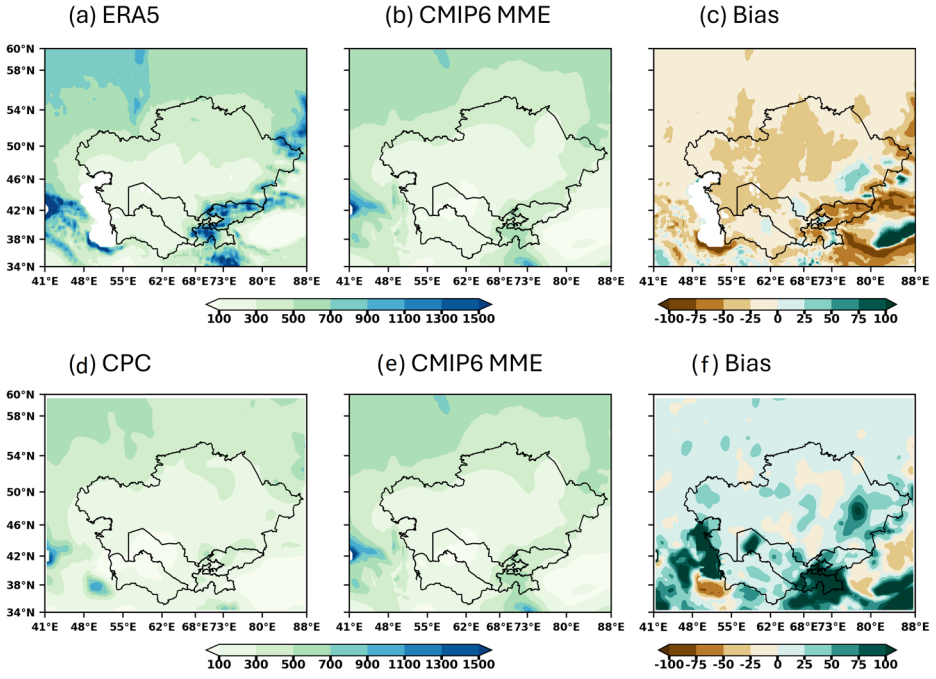

Fig. 4 Spatial distribution of mean ANP over CA during 1985–2014 (**a**) ERA5, (**b**) MME, (**c**) Bias (MME-ERA5), **d** (CPC), **e** (MME) and (**f**) bias (MME- CPC)

downscaled, bias-corrected datasets significantly reduced biases compared to the original CMIP6 datasets, with bias values typically falling within the range of ± 10% for most locations. These findings indicate that the MME offers a more dependable estimate of mean precipitation compared to individual models when evaluated against observations. In comparison, both the CPC and MME exhibit very similar spatial distributions of precipitation across the CA region (Fig. 4d and e). The MME closely simulated the precipitation across most arid regions of Uzbekistan, Turkmenistan, and the south-central parts of Kazakhstan, where mean annual rainfall ranged from 100 to 300 mm/year according to CPC data. In addition, the MME model captured similar amounts ranging from 150 to 400 mm/year. However, the MME overestimated the precipitation in the mountainous regions of CA and northeastern parts of Kazakhstan.

The analysis of historical precipitation data from the MME focused on evaluating its representation of extreme precipitation indices, including SDII, CDD, PD10MM, and RX1DAY. This comprehensive assessment compared the MME data with the gridded ERA5 product over a 30-year period from 1985 to 2014, presenting their relative biases in Supplementary Fig. 3. Throughout the evaluation, it was consistently observed that the MME historical simulation tends to underestimate PD10MM and SDII while overestimating CDD, particularly in regions of higher elevation where greater precipitation is typically observed. However, the MME exhibits reasonable performance in simulating one-day highest precipitation amounts (Supplementary Fig. 3K), showing similar characteristics to precipitation intensity. Regarding heavy precipitation days (PD10MM), the MME accurately captures occurrences in mountainous regions like Tajikistan and Kyrgyzstan, typically ranging between 15 and 20 days. Other dry areas experience fewer than five days (Supplementary Fig. 3h). The distribution of PD10MM during the period closely resembles observed data, although with a slight positive bias over plains and a negative bias over high altitudes. The MME generally overestimated the spatial pattern of CDD (Supplementary Fig. 3e), especially over arid regions such as Turkmenistan and central Uzbekistan. However, there is a slight underestimation of CDD in northern Kazakhstan and southeastern Kyrgyzstan, with the potential for further overestimation in other regions compared to observations. These findings instill confidence in suggesting that the NEX-GDDP CMIP6 dataset can effectively replicate the spatial patterns of precipitation extremes across Central Asia. Further comparison with the CPC dataset reveals that the MME tends to overestimate PD10MM, particularly in the high-altitude regions of Tajikistan and Kyrgyzstan. Additionally, daily rainfall intensity demonstrates significant spatial variability, with higher intensity observed over Tajikistan and Kyrgyzstan. As previously noted, the MME tends to overestimate CDD, particularly in the south-central parts of Central Asia, with a notable spatial extent over Turkmenistan and Uzbekistan (Fig. 5).

As per the above instigation, models perform very differently for various precipitation indices (Figs. 4 and 5; Supplementary Fig. 4). Therefore, a more thorough examination is necessary to evaluate the models' ability to simulate precipitation indices precisely. To pursue this goal, two additional metrics, namely Interannual Variability Skill (IVS) and Relative Error (RE), were utilized to evaluate model performance and corresponding indices over a 30-year period from 1985 to 2014. Initially, the IVS assessed how the models reproduce observed interannual variability. Furthermore, the relative error (RE) was utilized to validate each model's mean error. Accurately reproducing temporal variations is crucial in assessing model performance within the study region. The IVS values for ANP and

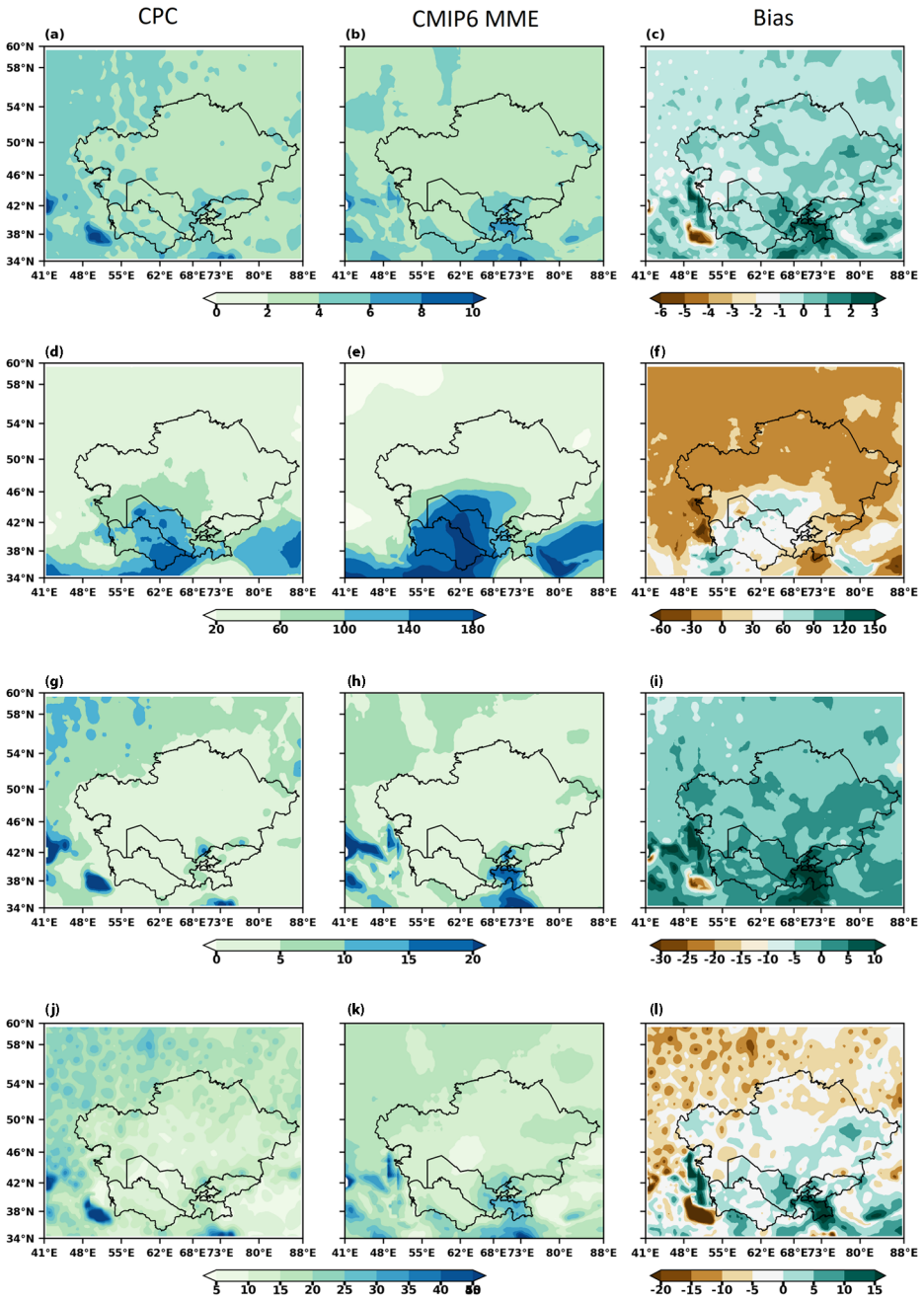

Fig. 5 The spatial distribution of extreme precipitation indices across CA is depicted in three columns: CPC (1st column), CMIP6 MME (2nd column), and BIAS (3rd column) for the period 1985–2014. Rows indicate extreme precipitation events, SDII (**a**, **b**, **c**), CDD (**d**, **e**, **f**), PD10MM (**g**, **h**, **i**) and RX1DAY (**j**, **k**, **l**)

indices across the CA are shown in Supplementary Fig. 4a, along with their MME equivalents for each model run. The IVS values of every grid point were first calculated and then averaged. The results show that CMIP6 models' capability to replicate intense precipitation varies consistently. Specifically, Supplementary Fig. 5a illustrates that most individual models revealed IVS values lower than 2.0 for annual rainfall amounts, CDD, and SDII. In comparison, the RX1DAY and PD10 MM IVS values were above 2.0. This variation among RX1DAY and PD10MM simulation contrasts with the MME's more reliable estimation of interannual variability. A reasonable simulation of observed interannual variability is shown by low IVS values, which are particularly noticeable in the MME for all precipitation indices except for PD10MM and RX1DAY.

The IVS values were particularly elevated for the CMIP6 models and CPC datasets, with ANP amounts ranging between 1.5 and 2.7. Similar results were noted for the PD10mm, CDD, and RX1DAY indices. However, IVS values for SDII were consistently below 2.1. Similarly, CMIP6 models and MME exhibited a consistent IVS in the SDII values, with the exception of a few models, which are primarily below 1.8. Higher IVS values, ranging from 1.8 to 4.9 and 1.6 to 3.9, respectively, were noted for extreme precipitation indices RX1DAY and PD10MM. In comparison, the MME consistently outperforms individual models in reproducing the interannual variability of ANP, highlighting its superior performance in this aspect. The MME's consistent and superior performance instills confidence in its reliability. The model's performance was further assessed to ascertain the Relative Error (RE) between ERA5/CPC gridded precipitation and CMIP6 models across CA (Supplementary Fig. 5b; Fig. 6b). The RE values indicate overestimated and underestimated precipitation indices based on positive and negative RE values. A RE value close to zero signifies a close alignment between the modelled and observed datasets. All CMIP6 models consistently underestimated ANP amounts, ranging between −25.4% to −31.7%, with the MME displaying −29% compared to ERA5 data. Conversely, CPC results consistently diverged from ERA5 datasets, with ANP amounts showing RE values ranging from −2.5% to −24.9% and the MME displaying a −16.2% RE (Fig. 6). In most cases, CMIP6 models underestimated precipitation indices, with MME RE values underestimated compared to ERA5 datasets. Particularly, RE of RX1DAY and PD10MM displayed −24% and −44%, respectively, while SDII exhibited < 10%. Furthermore, both CMIP6 models and the MME overestimated CDD, with RE values ranging from 30 to 44% compared with the ERA5 reanalysis, while it ranged from 8.6 to 20 compared with the CPC dataset.

3.3 Future projected changes in mean precipitation

The bias-corrected and statistically downscaled CMIP6 models revealed a consistent upward trend in annual mean precipitation across CA throughout the 20th and 21st centuries under various climate change scenarios (Fig. 7). Spatial patterns of the MME indicate an increase of up to 16% in the near future (2021–2050), notably over central Uzbekistan, southeastern Tajikistan, and southwestern Kyrgyzstan. This trend intensifies in the very high emission scenario (SSP5-8.5) compared to the historical period (1985–2014). The results further indicate a rise in precipitation levels in the mid and far future under SSP2-4.5, SSP3-7.0, and SSP5-8.5, particularly over Turkmenistan, Uzbekistan, Tajikistan, Kyrgyzstan, and southern and central regions of Kazakhstan. The most substantial increase was observed during the far future, under SSP3-7.0 and SSP5-8.5, with over a 50% rise in annual mean precipitation

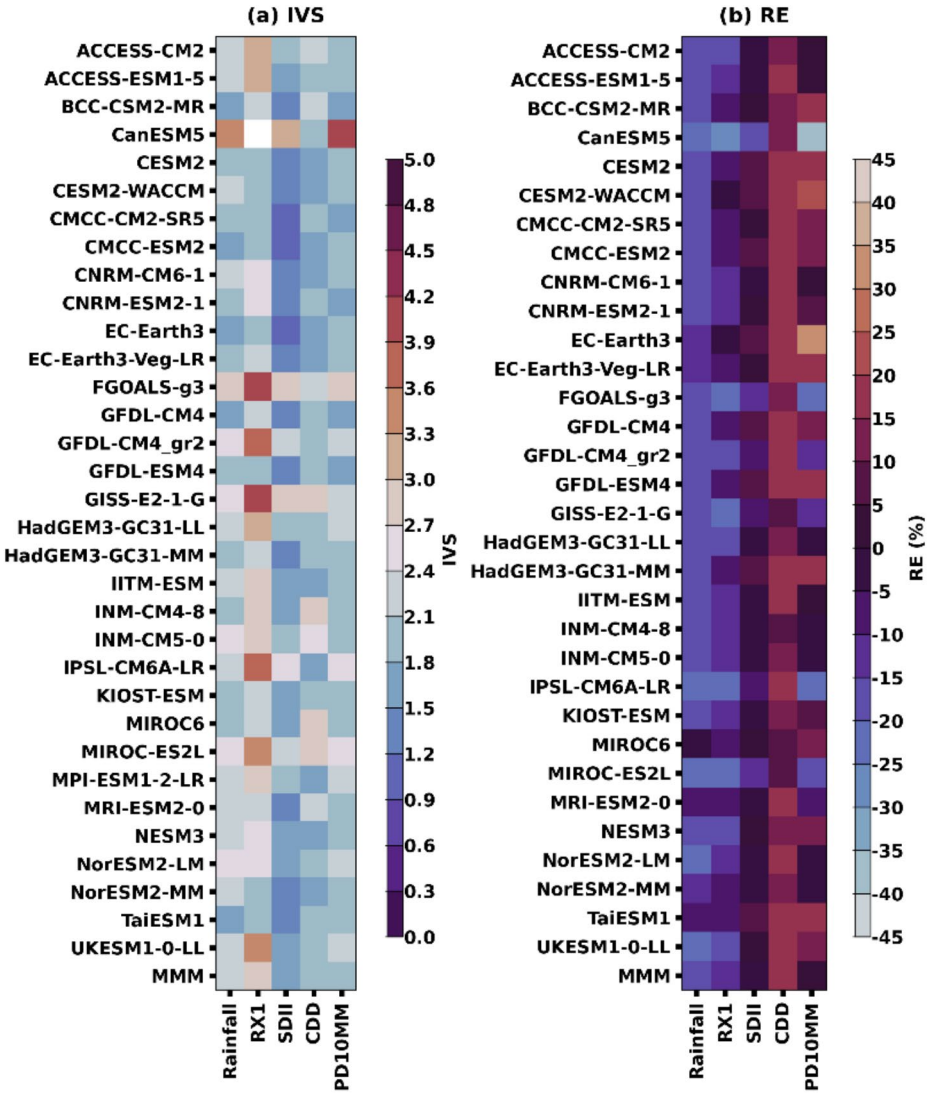

Fig. 6 Using CPC gridded precipitation data, a series of portrait diagrams showing the model performance of (**a**) Interannual Variability Score (IVS) and (**b**) Relative Error (RE), for precipitation extreme indices area-averaged over CA from 1985 to 2014

over southeastern CA (Fig. 7i and l). Equally, no significant change was observed across different time periods and SSPs in Northern Kazakhstan.

Under all the Shared Socioeconomic Pathways (SSPs), it is predicted that the average projected mean ANP across CA will increase by up to 33% during the mid-century compared to the historical period, especially over central Uzbekistan and the high altitudes of Tajikistan and Kyrgyzstan. While, in the near-future, the region's annual total precipitation will probably stay the same. Changes in atmospheric thermodynamics, circulation patterns, and heightened variability may contribute to wetter conditions than the present average

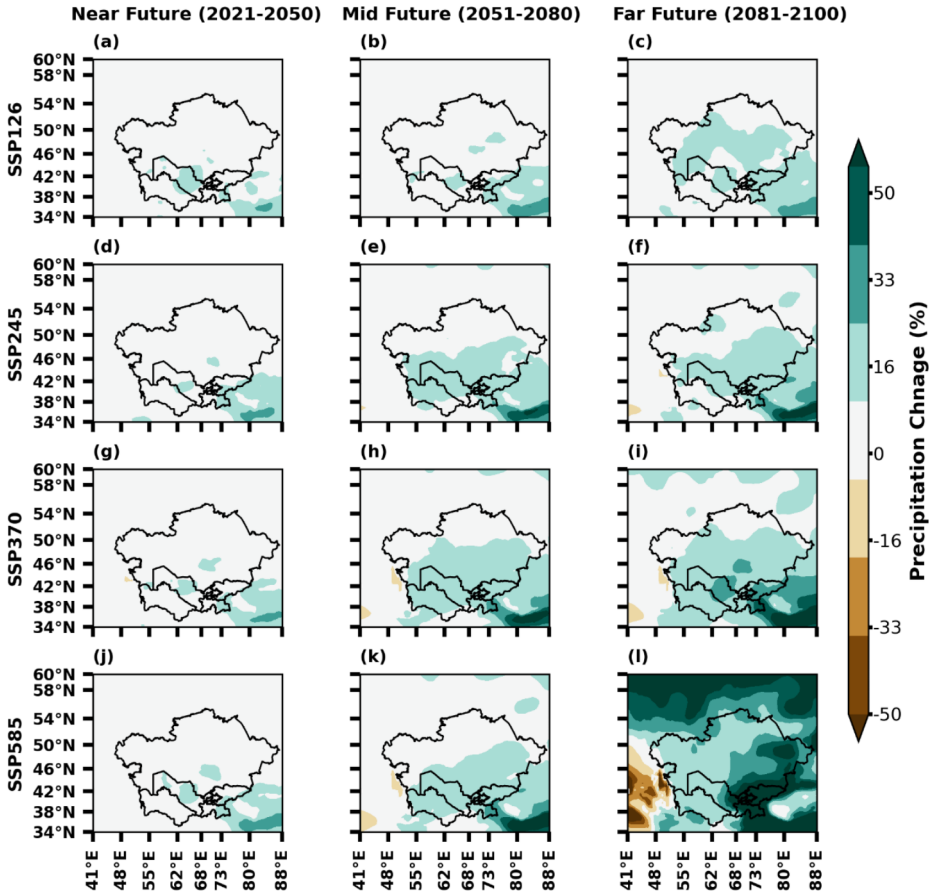

Fig. 7 The Projected changes in annual mean precipitation (%) across CA are examined under various climate change scenarios within the CMIP6 framework, spanning near (2021–2050), mid (2051–2080), and far future (2081–2100) timeframes, with reference to the baseline period (1985–2014)

precipitation. The mean precipitation over CA (area-weighted) is expected to rise by up to 25% in the future compared to the MME baseline, as shown in the Supplementary Fig. 6.

The temporal anomalies of mean ANP (area-weighted over the CA), depicted in Supplementary Fig. 6, reveal that both ERA5 and CPC exhibited relatively higher interannual variability compared to the MME historic precipitation anomalies. The mean ANP over CA throughout the historical period (1950–2014) was approximately 365 mm/year with a standard deviation of 6.7. In contrast, ERA5 and CPC illustrated 467 mm/year values and 282 mm/year, respectively. Precipitation quantities are expected to rise significantly during the 20th and 21st centuries across all four SSPs. These increasing trends in precipitation anomalies suggest a slight wetting tendency in the future. Specifically, in the near-future, precipitation amounts may range from 332 ± 6.3 mm to 345 ± 10.4 mm. Similarly, in the mid-future and far-future the range was projected to be 350 ± 6.5 mm to 354 ± 9.8 mm, and 354 ± 5.2 mm to 365 ± 8.6 mm, respectively. These changes in precipitation amounts represent possible ranges under different SSPs and time periods.

3.3.1 Projected changes in extreme precipitation indices

The analysis of projected changes in extreme precipitation indices compared to CMIP6 historic simulations provides insights into potential impacts on hydrological, agricultural systems, and society. Such investigations aid in developing tailored adaptation strategies to effectively address the adverse effects of extreme precipitation events resulting from global warming.

Supplementary Fig. 7 illustrates the expected percentage changes in simulated SDII relative to historical simulations. SDII is anticipated to increase across the CA under different SSPs and time periods. The MME predicts more frequent and intense SDII events across the CA by the end of the twenty-first century, with noticeable intensity in the far-future under SSP3-7.0 and SSP5-8.5, particularly over the mountainous regions of Uzbekistan, Tajikistan, and Kyrgyzstan. The estimated intensity shift is expected to range from −10 to 25% relative to the baseline, particularly in the mid and far future under SSP3-7.0 and SSP5-8.5. Across all scenarios, the near-future climate projection predicted less intensity in the CA region, with an increase of less than 5%. However, in the mid-term, strong precipitation events are expected to rise, particularly in the southeastern sections of CA, by more than 15%. Similarly, in the far future under all SSPs, intensity is expected to be significantly higher in SSP5-8.5, with an increase of above 25% for such events.

Further examination of changes in heavy precipitation days (>10 mm/day) revealed an upward trend across the CA (Supplementary Fig. 8). In the near future under different SSPs, these heavy precipitation days are anticipated to increase by 15–35% over Uzbekistan, particularly in the central lowlands extending towards the northwestern parts, and the south-central parts of Kazakhstan. During the mid-future, intensified heavy precipitation is projected to gradually increase from SSP1-2.6 to SSP5-8.5, exceeding 40%. This increase is primarily observed in the central region of CA, covering the northern parts of Turkmenistan, Uzbekistan, the central highlands of Kazakhstan, and the high altitudes of Tajikistan and Kyrgyzstan. The highest increase is noted in the far future, mostly under SSP3-7.0 and SSP5-8.5 across CA, exceeding 45%. These findings suggest that in the future, the CA region may experience a rise in heavy precipitation, particularly during wet periods, potentially contributing to the overall increase in ANP amounts under changing climatic conditions.

Understanding the frequency, intensity, and spatial distribution of the one-day highest precipitation amount (RX1DAY) is crucial for assessing potential impacts across various sectors. In CA, the projected increase in RX1DAY toward the end of the 21st century suggests a higher likelihood of intense precipitation events, raising concerns about more frequent and severe flooding, surface runoff, and soil degradation, which pose significant challenges for agriculture in the region (Supplementary Fig. 9). A projected increase in RX1DAY of up to 10% is anticipated across CA in the near future, particularly over mountainous regions. By the mid-future, intensified RX1DAY occurrences are expected in southern parts of CA, including Turkmenistan, Uzbekistan, Tajikistan, and Kyrgyzstan, as well as central and southern parts of Kazakhstan. By the end of the 21st century, a significant rise exceeding 30% is projected, indicating a substantial shift in precipitation patterns. The regional distribution of RX1DAY suggests that precipitation will become increasingly intense and less frequent in the future, with significant geographic variations across CA, highlighting the complexity and diversity of future precipitation trends in the region.

Projected changes in multi-year averages of Consecutive Dry Days (CDD) across Central Asia (CA) are summarized in Supplementary Fig. 10 under various SSPs and timeframes. During the historical period (1985–2014), the MME of CDD ranged from 20 to 180 days, with higher values in the south-central regions and lower values in northern and high-altitude areas. As an indicator of dryness and the length of dry spells, CDD suggests a mild dryness pattern across CA, with reductions of up to 6 days anticipated in the near future. In the mid-future, CDD increases become evident over Uzbekistan and Turkmenistan under SSP3-7.0 and SSP5-8.5. By the far future, under the high-emission scenario SSP5-8.5, CDD is expected to rise by up to 8 days, particularly in the highlands of Tajikistan, Kyrgyzstan, Uzbekistan, and western CA. Although general precipitation pattern changes are consistent across scenarios, variability intensifies with higher SSPs, with the most pronounced shifts occurring in SSP5-8.5. Most precipitation metrics show an increasing trend across CA in MME forecasts for the 21st century. Mean anomaly time series for historical simulations, observed data (CPC and ERA5), and modeled future precipitation indices averaged over CA are presented in the supplementary materials (Fig. 5; Supplementary Fig. 4).

4 Discussion

The dynamic shifts in spatially and temporally precipitation patterns exert detrimental effects on agricultural systems, water resources, hydroelectric power generation, and the environment at local and global scales (Abbas et al. 2021). Comparison of spatiotemporal simulation performance between CMIP6 models and MME with ERA5 and CPC reveals significant dry bias in most CMIP6 models across CA when contrasted with ERA5, consistent with other findings that noted ERA5's tendency to overestimate precipitation across CA by 20 to 60% (Song et al. 2022). Conversely, ERA5 overestimated low precipitation events while underestimated high-intensity precipitation and concluded ERA5's relatively poor performance in reproducing interannual variability over Asia (Dong and Dong 2022; Xin et al. 2022). The intricate nature of precipitation poses challenges for predicting and projecting future changes, which is crucial for understanding projected impacts and developing mitigation strategies for severe socio-economic consequences due to climate change. The complex geography of CA adds another layer of intricacy, with research suggesting distinct variations in precipitation patterns between its plains and mountainous regions (Hu et al. 2014, 2016). Topography plays a crucial role in shaping precipitation distribution, as seen in the spatial differences in precipitation levels (Li et al. 2020; Jin et al. 2024). Despite being widely used in arid CA, ERA5's accuracy falters in mountainous terrain (Li et al. 2022; Song et al. 2022), prompting the need to rely on two global gridded monthly datasets (CRU/GPCC). This approach becomes necessary due to sparse observational data in the region, helping better comprehend the spatial and temporal variations in precipitation. Precipitation data sourced from global precipitation products are paramount for data-scarce or ungauged regions, such as CA.

Alternatively, while gauge-based CPC precipitation tends to underestimate precipitation amounts across CA, it adeptly captures spatial distribution, particularly notable in plains (Dilinuer et al. 2021). Across various time scales (daily, monthly, yearly), ERA5 generally outperforms CPC in capturing precipitation patterns across both plains and mountainous regions. Access to precipitation data from global sources is crucial for regions with limited

data availability, such as CA, due to the scarcity of weather station data and variations in interpolation methods. ERA5 performs well in regions with sufficient precipitation but poorly in mountainous and high-altitude areas. Simulating precipitation in such regions, particularly the Tian Shan and Pamir mountains, is challenging (Zhang et al. 2020; Hu and Yuan 2021). Additionally, ERA5 underperforms on wet and extremely wet days, as extremely heavy precipitation involves complex mechanisms and variable processes (Alexander et al. 2020; Bador et al. 2020; Dai and Nie 2020; Nguyen et al. 2020). Reanalysis datasets, including ERA5, exhibit significant uncertainties in capturing extremely heavy precipitation (Huang et al. 2016). Consequently, different global gridded precipitation products yield varying results in California (Schiemann et al. 2008). However, CMIP6 models and MME exhibit a strong negative bias, particularly in consecutive dry days (CDD) and maximum 1-day precipitation (RX1DAY), while overestimating mean and variability of extreme precipitations such as SDII and the count of heavy precipitation days (PD10MM). Similar overestimation tendencies of CMIP6 models were observed in East Africa and contiguous regions of the United States (Srivastava et al. 2020; Akinsanola et al. 2021). Higher resolution models show advantages in simulating extreme precipitation, especially in regions with complex topography (Luo and Guo 2022), where extreme precipitation is closely linked to convection and cloud microphysics (Keupp et al. 2019), complicating attribution of simulation differences among models across different global regions. The CA displayed an increase in ANP amounts across the time periods (near, mid, and far-future) under different SSP scenarios. The variability in precipitation changes across models is greater for higher emission scenarios. This can be partially attributed to the increased uncertainty in surface air temperature changes associated with higher radiation forcing (Roe and Baker 2007; Zhou and Xiaolong 2015). Moreover, examining changes in extreme precipitation indices reveals a general trend towards increased intensity as radiative forcing increases. These indices, including SDII, CDD, RX1DAY, and PD10MM, represent cumulative precipitation from heavy rainfall events and their contribution to ANP totals. Notably, discernible anthropogenic influences are evident in these extreme indices. Analysing long-term shifts in precipitation-based metrics, as employed here, offers a sophisticated perspective distinct from that of ANP alone. It captures the Consolidated impact of alterations in both the frequency and intensity of heavy rainfall occurrences. However, this analytical advantage is tempered by a significant challenge: disentangling the effects of frequency changes from intensity alterations proves intricate. Establishing a straightforward relationship between these indices and global warming levels becomes notably complex. For instance, while changes in RX1DAY closely adhere to the Clausius–Clapeyron relationship in observations and model simulations, elucidated by various studies (Westra et al. 2013; Li et al. 2020; Yao et al. 2021), pinpointing causality remains challenging. Recent research by (Yao et al. 2021; Zhang et al. 2022) indicates that the escalation in total ANP primarily stems from the intensification of extreme precipitation events, concurrent with the attenuation of lighter precipitation. This phenomenon leads to an overcompensation of increased evaporation due to concurrent global warming trends.

5 Summary and concluding remarks

This study used ERA5 reanalysis, CPC daily precipitation data, and 33 CMIP6 models from NASA's NEX-GDDP, downscaled to 0.25° × 0.25°, to analyze extreme precipitation indices in Central Asia. Most models accurately captured the spatial patterns of mean ANP, though RMSE values varied by dataset, with higher errors against ERA5 data, particularly in mountainous areas. The MME generally underestimated indices PD10MM and SDII while overestimating CDD, especially in high-altitude regions, with inconsistent performance across indices like PD10MM and RX1DAY. By the century's end, under all SSPs, APN is projected to increase up to 50%, with extreme events intensifying, particularly under SSP5-8.5, where SDII could rise over 25%, indicating a shift to wetter conditions, more heavy rainfall, and fewer dry days in parts of Central Asia. High-resolution data is essential for accurately understanding these changes, especially in climate-sensitive areas influenced by local factors; this analysis supports future impact studies and informs adaptation and mitigation policies for the region.

Supplementary Information The online version contains supplementary material available at https://doi.org/10.1007/s10584-025-03872-0.

Acknowledgements The authors wish to acknowledge the contribution of the International Center for Biosaline (ICBA) high-performance computing and research computing facilities to the results of this research. We would like to thank the editor and the two reviewers for their several constructive and insightful comments and suggestions that helped to substantially improve the quality of this manuscript.

Author contributions S.G. conceptualized the study, downloaded, and analysed the observational and modelled data with inputs from Both S.S and A.L.L authors wrote the manuscript.
Correspondence and requests for materials should be addressed to S.G.

Funding Funding was received from the core donors, the UAE government and the Islamic Development Bank (IsDB), on Climate Change impacts in both MENA and Central Asia regions (Project code ICBA082).

Data availability The observational and reanalysis products referenced in this study are readily accessible online: (1) ERA5, the fifth-generation climate reanalysis data, is accessible via the European Centre for Medium-Range Weather Forecasts (ECMWF) website; (2) The Climate Prediction Center (CPC) offers a dataset created through optimal interpolation of quality-controlled gauge records from the Global Telecommunication System (GTS) network on their website; (3) Simulated daily high-resolution statistically downscaled precipitation data was sourced from the NASA Earth Exchange Global Daily Downscaled Projections data portal; and (4) All figures were produced using Python Language software version 3.12.3.

Code availability The scripts utilized for processing all observational and modelled datasets are available upon reasonable request from the corresponding author at s.gummadi@biosaline.org.ae.

Declarations

Conflicts of interest The authors declare no conflicts of interest.

References

Abbas A, Waseem M, Ullah W et al (2021) Spatiotemporal analysis of meteorological and hydrological droughts and their propagations. Water (Switzerland) 13. https://doi.org/10.3390/w13162237

Aerenson T, Tebaldi C, Sanderson B, Lamarque JF (2018) Changes in a suite of indicators of extreme temperature and precipitation under 1.5 and 2 degrees warming. Environ Res Lett 13. https://doi.org/10.1088/1748-9326/aaafd6

Agel L, Barlow M, Polonia J, Coe D (2020) Simulation of Northeast U.S. Extreme Precipitation and its Associated circulation by CMIP5 models. J Clim 33:9817–9834. https://doi.org/10.1175/JCLI-D-19

Akinsanola AA, Ongoma V, Kooperman GJ (2021) Evaluation of CMIP6 models in simulating the statistics of extreme precipitation over Eastern Africa. Atmos Res 254. https://doi.org/10.1016/j.atmosres.2021.105509

Alexander LV, Zhang X, Peterson TC et al (2006) Global observed changes in daily climate extremes of temperature and precipitation. J Geophys Res Atmos 111. https://doi.org/10.1029/2005JD006290

Alexander LV, Bador M, Roca R et al (2020) Intercomparison of annual precipitation indices and extremes over global land areas from in situ, space-based and reanalysis products. Environ Res Lett 15. https://doi.org/10.1088/1748-9326/ab79e2

Avila-Diaz A, Abrahão G, Justino F et al (2020) Extreme climate indices in Brazil: evaluation of downscaled earth system models at high horizontal resolution. Clim Dyn 54:5065–5088. https://doi.org/10.1007/s00382-020-05272-9

Ayugi B, Jiang Z, Iyakaremye V et al (2022) East African population exposure to precipitation extremes under 1.5 °c and 2.0 °c warming levels based on CMIP6 models. Environ Res Lett 17. https://doi.org/10.1088/1748-9326/ac5d9d

Bador M, Alexander LV, Contractor S, Roca R (2020) Diverse estimates of annual maxima daily precipitation in 22 state-of-the-art quasi-global land observation datasets. Environ Res Lett 15. https://doi.org/10.1088/1748-9326/ab6a22

Becker A, Finger P, Meyer-Christoffer A et al (2013) A description of the global land-surface precipitation data products of the Global Precipitation Climatology Centre with sample applications including centennial (trend) analysis from 1901-present. Earth Syst Sci Data 5:71–99. https://doi.org/10.5194/essd-5-71-2013

Brunner L, Pendergrass AG, Lehner F et al (2020) Reduced global warming from CMIP6 projections when weighting models by performance and independence. Earth Sys Dyn 11:995–1012. https://doi.org/10.5194/esd-11-995-2020

Carter TR, Benzie M, Campiglio E et al (2021) A conceptual framework for cross-border impacts of climate change. Glob Environ Change. https://doi.org/10.1016/j.gloenvcha.2021.102307. 69:

Chen M, Shi W, Xie P et al (2008) Assessing objective techniques for gauge-based analyses of global daily precipitation. J Geophys Res Atmos 113. https://doi.org/10.1029/2007JD009132

Chevallier P, Pouyaud B, Mojaïsky M et al (2014) River flow regime and snow cover of the Pamir Alay (Central Asia) in a changing climate. Hydrol Sci J 59:1491–1506. https://doi.org/10.1080/02626667.2013.838004

Dai P, Nie J (2020) A global quasigeostrophic diagnosis of extratropical extreme precipitation. J Clim 33:9629–9642. https://doi.org/10.1175/JCLI-D-20-0146.1

Dilinuer T, Yao J, Chen J et al (2021) Systematical evaluation of three Gridded Daily Precipitation products against rain gauge observations over Central Asia. Front Earth Sci (Lausanne) 9. https://doi.org/10.3389/feart.2021.699628

Donat MG, Alexander LV, Yang H et al (2013) Global land-based datasets for monitoring climatic extremes. Bull Am Meteorol Soc 94:997–1006. https://doi.org/10.1175/BAMS-D-12-00109.1

Donat MG, Alexander LV, Herold N, Dittus AJ (2016) Temperature and precipitation extremes in century-long gridded observations, reanalyses, and atmospheric model simulations. J Geophys Res 121:11174–11189. https://doi.org/10.1002/2016JD025480

Dong T, Dong W (2022) AEvaluation of extreme precipitation over Asia in CMIP6 models evaluation of extreme precipitation over Asia in CMIP6 models. 57:1751–1769. https://doi.org/10.1002/essoar.10508599.1

Du Y, Wang D, Zhu J et al (2022) Comprehensive assessment of CMIP5 and CMIP6 models in simulating and projecting precipitation over the global land. Int J Climatol 42:6859–6875. https://doi.org/10.1002/joc.7616
Fallah B, Russo E, Menz C et al (2023) Anthropogenic influence on extreme temperature and precipitation in Central Asia. Sci Rep 13. https://doi.org/10.1038/s41598-023-33921-6
Fan Y, van den Dool H (2008) A global monthly land surface air temperature analysis for 1948-present. J Geophys Res Atmos 113. https://doi.org/10.1029/2007JD008470
Gleckler PJ, Taylor KE, Doutriaux C (2008) Performance metrics for climate models. J Geophys Res Atmos. https://doi.org/10.1029/2007JD008972. 113:
Goudie Andrew S (1994) Deserts in a warmer world. In: Millington AC KPyeW (ed) Environmental change in drylands: Biogeographical and Geomorphological perspectives, 4th edn. Wiley, New York, pp 1–29
Gusain A, Ghosh S, Karmakar S (2020) Added value of CMIP6 over CMIP5 models in simulating Indian summer monsoon rainfall. Atmos Res 232. https://doi.org/10.1016/j.atmosres.2019.104680
Harris I, Jones PD, Osborn TJ, Lister DH (2014) Updated high-resolution grids of monthly climatic observations - the CRU TS3.10 dataset. Int J Climatol 34:623–642. https://doi.org/10.1002/joc.3711
Harrison L, Funk C, Peterson P (2019) Identifying changing precipitation extremes in Sub-saharan Africa with gauge and satellite products. Environ Res Lett 14. https://doi.org/10.1088/1748-9326/ab2cae
Hersbach H, Bell B, Berrisford P et al (2020) The ERA5 global reanalysis. Q J R Meteorol Soc 146:1999–2049. https://doi.org/10.1002/qj.3803
Hu X, Yuan W (2021) Evaluation of ERA5 precipitation over the eastern periphery of the tibetan plateau from the perspective of regional rainfall events. Int J Climatol 41:2625–2637. https://doi.org/10.1002/joc.6980
Hu Z, Zhang C, Tian H (2014) Temperature changes in Central Asia from 1979 to 2011 based on multiple Datasets*. J Clim 27:1143–1167. https://doi.org/10.1175/JCLI-D-13
Hu Z, Hu Q, Zhang C et al (2016) Evaluation of reanalysis, spatially interpolated and satellite remotely sensed precipitation data sets in central Asia. J Geophys Res 121:5648–5663. https://doi.org/10.1002/2016JD024781
Huang DQ, Zhu J, Zhang YC et al (2016) Assessment of summer monsoon precipitation derived from five reanalysis datasets over East Asia. Q J R Meteorol Soc 142:108–119. https://doi.org/10.1002/qj.2634
IPCC (2022) Summary for Policymakers. In: (IPCC) IP on CC (ed) Global warming of 1.5°C: IPCC special report on impacts of global warming of 1.5°C above pre-industrial levels in context of strengthening response to climate change, sustainable development, and efforts to eradicate poverty. Cambridge University Press, Cambridge, pp 1–24
Jain S, Salunke P, Mishra SK et al (2019) Advantage of NEX-GDDP over CMIP5 and CORDEX Data: Indian summer Monsoon. Atmos Res 228:152–160. https://doi.org/10.1016/j.atmosres.2019.05.026
Jin C, Wang B, Cheng TF et al (2024) How much we know about precipitation climatology over Tianshan Mountains—the central Asian water tower. NPJ Clim Atmos Sci 7. https://doi.org/10.1038/s41612-024-00572-x
Kendall MG (1975) Rank correlation methods, 4th edn. Charles Griffin, London
Kenzhebaev R, Barandun M, Kronenberg M et al (2017) Mass balance observations and reconstruction for Batysh Sook Glacier, Tien Shan, from 2004 to 2016. Cold Reg Sci Technol 135:76–89. https://doi.org/10.1016/j.coldregions.2016.12.007
Keupp L, Hertig E, Kaspar-Ott I et al (2019) Weighted multi-model ensemble projection of extreme precipitation in the Mediterranean region using statistical downscaling. Theor Appl Climatol 138:1269–1295. https://doi.org/10.1007/s00704-019-02851-7
Kim YH, Min SK, Zhang X et al (2016) Attribution of extreme temperature changes during 1951–2010. Clim Dyn 46:1769–1782. https://doi.org/10.1007/s00382-015-2674-2
Li Z, Chen Y, Li W et al (2015) Potential impacts of climate change on vegetation dynamics in Central Asia. J Geophys Res 120. https://doi.org/10.1002/2015JD023618. 12.345-12,356
Li Y, Chen Y, Li Z (2020) Climate and topographic controls on snow phenology dynamics in the Tienshan Mountains, Central Asia. Atmos Res 236. https://doi.org/10.1016/j.atmosres.2019.104813
Li Y, Qin X, Liu Y et al (2022) Evaluation of long-term and high-resolution Gridded Precipitation and Temperature products in the Qilian Mountains, Qinghai–Tibet Plateau. Front Environ Sci 10. https://doi.org/10.3389/fenvs.2022.906821
Lioubimtseva E, Cole R (2006) Uncertainties of climate change in arid environments of Central Asia. Rev Fish Sci Aquac 14(1–2):29–49
Lioubimtseva E, Henebry GM (2009) Climate and environmental change in arid Central Asia: impacts, vulnerability, and adaptations. J Arid Environ 73:963–977
Lioubimtseva E, Simon B, Faure H et al (1998) Impacts of climatic change on carbon storage in the Sahara-Gobi. desert belt since the Last Glacial Maximum

Liu Z, Huang J, Xiao X, Tong X (2022) The capability of CMIP6 models on seasonal precipitation extremes over Central Asia. Atmos Res 278. https://doi.org/10.1016/j.atmosres.2022.106364
Luo N, Guo Y (2022) Impact of model resolution on the simulation of precipitation extremes over China. Sustain (Switzerland) 14. https://doi.org/10.3390/su14010025
Maurer EP, Hidalgo HG (2008) Hydrology and Earth System sciences Utility of daily vs. monthly large-scale climate data. an intercomparison of two statistical downscaling methods
McMahon TA, Peel MC, Karoly DJ (2015) Assessment of precipitation and temperature data from CMIP3 global climate models for hydrologic simulation. Hydrol Earth Syst Sci 19:361–377. https://doi.org/10.5194/hess-19-361-2015
Narbayep M, Pavlova V (2022) The Aral Sea, Central Asian countries and climate change in the 21st century. Bangkok
Nguyen PL, Bador M, Alexander LV et al (2020) On the robustness of Annual Daily Precipitation Maxima estimates over Monsoon Asia. Front Clim 2:1–19. https://doi.org/10.3389/fclim.2020.578785
Roe GH, Baker MB (2007) Why is climate sensitivity so unpredictable? Science (1979) 318:629–632. https://doi.org/10.1126/science.1144735
Scherrer SC (2011) Present-day interannual variability of surface climate in CMIP3 models and its relation to future warming. Int J Climatol 31:1518–1529. https://doi.org/10.1002/joc.2170
Schiemann R, Lüthi D, Vidale PL, Schär C (2008) The precipitation climate of Central Asia - Intercomparison of observational and numerical data sources in a remote semiarid region. Int J Climatol 28:295–314. https://doi.org/10.1002/joc.1532
Sen PK (1968) Estimates of the regression coefficient based on Kendall's tau. J Am Stat Assoc 63:1379–1389. https://doi.org/10.1080/01621459.1968.10480934
Sillmann J, Kharin VV, Zhang X et al (2013a) Climate extremes indices in the CMIP5 multimodel ensemble: part 1. Model evaluation in the present climate. J Geophys Res Atmos 118:1716–1733. https://doi.org/10.1002/jgrd.50203
Sillmann J, Kharin VV, Zwiers FW et al (2013b) Climate extremes indices in the CMIP5 multimodel ensemble: part 2. Future climate projections. J Geophys Res Atmos 118:2473–2493. https://doi.org/10.1002/jgrd.50188
Song L, Xu C, Long Y et al (2022) Performance of seven Gridded Precipitation products over Arid Central Asia and subregions. Remote Sens (Basel) 14. https://doi.org/10.3390/rs14236039
Srivastava A, Grotjahn R, Ullrich PA (2020) Evaluation of historical CMIP6 model simulations of extreme precipitation over contiguous US regions. Weather Clim Extrem 29. https://doi.org/10.1016/j.wace.2020.100268
Stott P (2016) How climate change affects extreme weather events. Sci (1979) 352:1517–1518. https://doi.org/10.1126/science.aaf7271
Ta Z, Yu Y, Sun L et al (2018) Assessment of precipitation simulations in Central Asia by CMIP5 climate models. Water (Switzerland) 10. https://doi.org/10.3390/w10111516
Thrasher B, Maurer EP, McKellar C, Duffy PB (2012) Technical note: Bias correcting climate model simulated daily temperature extremes with quantile mapping. Hydrol Earth Syst Sci 16:3309–3314. https://doi.org/10.5194/hess-16-3309-2012
Thrasher B, Wang W, Michaelis A et al (2022) NASA Global Daily Downscaled projections, CMIP6. https://doi.org/10.1038/s41597-022-01393-4. Sci Data 9:
Varushenko SIVAN and KRK (1987) Changing of the Caspian Sea regime and enclosed basins in geological time. Moscow, Nauka, Russia, p 240
Westra S, Alexander LV, Zwiers FW (2013) Global increasing trends in annual maximum daily precipitation. J Clim 26:3904–3918. https://doi.org/10.1175/JCLI-D-12-00502.1
Wilson AB, Avila-Diaz A, Oliveira LF et al (2022) Climate extremes and their impacts on agriculture across the Eastern Corn Belt Region of the U.S. Weather Clim Extrem 37. https://doi.org/10.1016/j.wace.2022.100467
Wood AW, Maurer EP, Kumar A, Lettenmaier DP (2002) Long-range experimental hydrologic forecasting for the eastern United States. J Geophys Research: Atmos 107. https://doi.org/10.1029/2001JD000659. ACL 6-1-ACL 6–15
Wood AW, Leung LR, Sridhar V, Lettenmaier DP (2004) Hydrologic implications of dynamical and statistical approaches to downscaling climate model outputs
Xin Y, Yang Y, Chen X et al (2022) Evaluation of IMERG and ERA5 precipitation products over the Mongolian Plateau. Sci Rep 12. https://doi.org/10.1038/s41598-022-26047-8
Xu L, Zhang T, Yu W, Yang S (2023) Changes in concurrent precipitation and temperature extremes over the Asian monsoon region: observation and projection. Environ Res Lett 18. https://doi.org/10.1088/1748-9326/acbfd0

Xu L, Yu W, Yang S, Zhang T (2024) Concurrent drought and heatwave events over the Asian monsoon region: insights from a statistically downscaling CMIP6 dataset. Environ Res Lett 19. https://doi.org/10.1088/1748-9326/ad2cad

Yao J, Chen Y, Chen J et al (2021) Intensification of extreme precipitation in arid Central Asia. J Hydrol (Amst) 598. https://doi.org/10.1016/j.jhydrol.2020.125760

YIN H, SUN Y (2018) Characteristics of extreme temperature and precipitation in China in 2017 based on ETCCDI indices. Adv Clim Change Res 9:218–226. https://doi.org/10.1016/j.accre.2019.01.001

Zhang X, Wan H, Zwiers FW et al (2013) Attributing intensification of precipitation extremes to human influence. Geophys Res Lett 40:5252–5257. https://doi.org/10.1002/grl.51010

Zhang M, Chen Y, Shen Y, Li B (2019) Tracking climate change in Central Asia through temperature and precipitation extremes. J Geog Sci 29:3–28. https://doi.org/10.1007/s11442-019-1581-6

Zhang L, Ren D, Nan Z et al (2020) Interpolated or satellite-based precipitation? Implications for hydrological modeling in a meso-scale mountainous watershed on the Qinghai-Tibet Plateau. J Hydrol (Amst) 583:124629. https://doi.org/10.1016/j.jhydrol.2020.124629

Zhang X, Chen Y, Fang G et al (2022) Observed changes in extreme precipitation over the Tienshan Mountains and associated large-scale climate teleconnections. J Hydrol (Amst) 606:127457. https://doi.org/10.1016/j.jhydrol.2022.127457

Zhou T, Xiaolong C (2015) Uncertainty in the 2°C warming threshold related to Climate Sensitivity and Climate Feedback. J METEOROLOGICAL Res 29:884–895. https://doi.org/10.1007/s13351